Luminescence spectroscopy and NIR to VIS upconversion of Cs_2GeF_6: 2% Re^{4+}

2001 J. Phys.: Condens. Matter 13 9583

(http://iopscience.iop.org/0953-8984/13/42/317)

INSTITUTE OF PHYSICS PUBLISHING JOURNAL OF PHYSICS: CONDENSED MATTER

J. Phys.: Condens. Matter **13** (2001) 9583–9598 PII: S0953-8984(01)24245-3

Luminescence spectroscopy and NIR to VIS upconversion of Cs_2GeF_6: 2% Re^{4+}

Markus Wermuth and Hans U Güdel

Departement für Chemie und Biochemie, Universität Bern, Freiestrasse 3, 3000 Bern 9, Switzerland

Received 25 April 2001, in final form 2 July 2001
Published 5 October 2001
Online at stacks.iop.org/JPhysCM/13/9583

Abstract

We present and analyse high-resolution absorption, luminescence and upconversion-luminescence spectra of Cs_2GeF_6: 2% Re^{4+}. The crystals of Cs_2GeF_6: 2% Re^{4+} were grown from solution. Upon excitation around 11 000 cm^{-1} in the near infrared, visible upconversion luminescence around 17 000 cm^{-1} is observed. On increasing the temperature from 15 K to room temperature the integrated upconversion luminescence intensity decreases to 2%. This is attributed to the decreasing absorption cross-section at the monochromatic laser-excitation energy. The upconversion excitation spectra and the results obtained from time-dependent measurements indicate a dominant energy-transfer upconversion mechanism.

1. Introduction

The photophysical phenomenon of upconversion luminescence is based on the sequential absorption of low-energy photons, leading to the emission of high-energy photons [1]. A common prerequisite for the various upconversion mechanisms described in the literature is the availability of more than one metastable excited state. This explains, why the majority of upconversion systems investigated so far contain rare-earth ions, in which the well shielded f-electrons give rise to multiple luminescent excited states. Besides fundamental research aspects, the investigation of new upconversion systems is driven by their application potential as upconversion phosphors and upconversion-laser materials. In this materials-oriented research, fluorides and oxides are the most frequently used host crystals and glasses, due to their favourable chemical, physical and mechanical properties. The major drawback of oxides and fluorides, compared to the heavier halides, relates to their relatively high phonon energies, which leads to enhanced non-radiative relaxation of excited states that are separated by only small energy gaps from lower electronic states.

In recent years, we have explored the upconversion-research field along two chemical coordinates: (i) First, we have expanded the upconversion research towards the rare-earth ion doped heavier halide hosts that are characterized by lower phonon energies. This has

turned out to be very rewarding in that non-radiative relaxation losses have been successfully reduced, thus opening the way for new upconversion processes [2, 3]. (ii) More recently, we have extended our upconversion research towards transition-metal ions [4] that differ from lanthanide ions by their increased d–d oscillator strengths, broader luminescence bands and larger chemical tuning potential. These advantageous properties are intrinsically related to stronger electron–phonon coupling, though, making non-radiative multiphonon relaxation the predominant relaxation process for most of the excited states. As Kasha realized decades ago [5], usually only the lowest excited states give rise to luminescence in transition-metal ion doped compounds. Therefore, the number of transition-metal ions showing higher excited state luminescence is small. So far, we have reported on upconversion of Ti^{2+} [6], Ni^{2+} [7–9], Mo^{3+} [10, 11], Re^{4+} [10, 12] and Os^{4+} [13, 14] doped halide lattices. Among these systems, Cs_2ZrCl_6: Re^{4+} turned out to be a remarkably efficient upconversion system up to room temperature, and possible laser operating schemes were proposed on the basis of the promising spectroscopic results [12].

In this report, we present high-resolution absorption, luminescence and upconversion-luminescence spectra of Cs_2GeF_6: 2% Re^{4+}. Cs_2GeF_6 crystallizes in the cubic space group *Fm3m* is thus isostructural to $Cs_2\,ZrCl_6$ and offers perfectly octahedral sites for Re^{4+}. From the analysis of the results obtained from CW and dynamic spectroscopic experiments at variable temperatures, we gain detailed information on the relevant upconversion mechanisms and on possible excitation-loss processes. By demonstrating the feasibility of Re^{4+} upconversion in a fluoride environment, we open the door for more materials-oriented research.

2. Experimental procedure

2.1. Synthesis and crystal growth

K_2ReF_6 was synthesized from K_2ReBr_6 using KHF_2 as a fluorinating agent [15]. The K_2ReF_6 thus obtained was slightly pink. Cs_2GeF_6 was prepared by dissolving GeO_2 in HF (20%) under heating, followed by precipitation with a solution of CsF in HF (20%). Crystals of Cs_2GeF_6: Re^{4+} were grown at room temperature by slow evaporation from a HF (10%) solution containing the appropriate amounts of Cs_2GeF_6 and K_2ReF_6. The actual Re^{4+} concentration in the crystal was estimated from absorption spectra assuming an identical $\int \epsilon(\nu)\,\mathrm{d}\nu = 28\mathrm{l\ mol^{-1}\,cm^{-2}}$ for the absorption line around 17 900 $\mathrm{cm^{-1}}$ in Cs_2GeF_6: Re^{4+} and K_2ReF_6. The Re^{4+} concentration in the crystal was typically found to be 30% of the concentration in solution. A Cs_2GeF_6: 2% Re^{4+} crystal was used for the following spectroscopic experiments.

2.2. Spectroscopic measurements

Absorption spectra were recorded on a Cary 5e (Varian) spectrometer, using a closed-cycle cryostat (Air Products) for cooling the sample crystal.

Upconversion and near-infrared (NIR) luminescence spectra were obtained by using an argon-ion laser (Spectra Physics 2060-10SA) pumped Ti:Sapphire laser (Spectra Physics 3900S) as a tunable excitation source. Wavelength control was achieved by an inchworm (Burleigh PZ 501) driven birefringent filter. The visible (VIS) luminescence was excited by the 514.5 nm (19 430 $\mathrm{cm^{-1}}$) line of the Ar^+ laser, dispersed by a 0.85 m double monochromator (Spex 1402) and detected by a cooled photomultiplier (RCA C31034), using a photon-counting system (Stanford Research 400). NIR luminescence was dispersed by a 0.75 m single monochromator (Spex 1702) and detected with a liquid-nitrogen cooled germanium

photodiode (ADC 403L) combined with a lock-in amplifier (Stanford Research 830). The samples were cooled with a quartz He flow-tube. Luminescence spectra were corrected for the sensitivity of the detection system and are displayed as photon flux versus energy.

The Γ_7 ($^2T_{2g}$) luminescence lifetime was determined after pulsed 18 653 cm^{-1} excitation with the anti-Stokes Raman shifted output (Quanta Ray RS-1, H_2 340 psi) of a dye laser (Lambda Physik FL3002, Pyridine 1 in methanol) pumped with the frequency doubled output of a Nd:YAG (yttrium aluminum garnet) laser (Quanta Ray DCR 3, 20 Hz). The sample luminescence was detected with the same PM tube and recorded with a multichannel scaler (Stanford Research 430). The Γ_7 ($^2T_{2g}$) upconversion-luminescence transient was excited with the experimental set-up described above, using the Stokes-shifted output at 11 429 cm^{-1} of the dye laser (DCM in methanol). The Γ_8 ($^2T_{1g}$) luminescence lifetime was determined after the same pulsed excitation. The NIR luminescence decay was detected with a fast Ge detector (ADC 403 HS, 1 μs response) and recorded using an oscilloscope (Tektronix TDS 540A).

3. Results

Figures 1(a) and (b) show two relevant parts of the absorption spectrum of Cs_2GeF_6: 2% Re^{4+} at $T = 15$ K. According to reference [16], the weak and sharp lines are assigned to Γ_7 ($^2T_{2g}$), Γ_8 ($^2T_{2g}$) in figure 1(a) and to Γ_8($^2T_{1g}$), Γ_8(^2E_g) and Γ_6 ($^2T_{1g}$) in figure 1(b). 0–0 and ν_6 (t_{2u}) ν_4 (t_{1u}) and ν_3 (t_{1u}) designate electronic and vibronic origins, respectively. The corresponding energy-level diagram with origin energies on the right is shown in figure 2.

Exciting Cs_2GeF_6: 2% Re^{4+} at 19 430 cm^{-1} at 15 K leads to the luminescence spectrum shown in figure 3(a). 0–0 indicates the position of the electronic origin of the Γ_7 ($^2T_{2g}$) $\rightarrow$ Γ_8 ($^4A_{2g}$) luminescence transition and ν_i ($i = 6, 4, 3$) label vibronic origins. The first members of the progressions in the ν_5 (t_{2g}) and ν_2 (e_g) modes on the electronic and vibronic origins are indicated. Figure 3(b) shows the Γ_8 ($^2T_{1g}$) $\rightarrow$ Γ_8 ($^4A_{2g}$) NIR luminescence of Cs_2GeF_6: 2% Re^{4+} excited at 10 804 cm^{-1} at $T = 15$ K. The electronic and vibronic origins are labelled, and the first members of progressions in the ν_5 (t_{2g}) and ν_2 (e_g) modes, respectively, on the electronic and vibronic origins are indicated. The energies of the luminescence lines observed in figures 3(a) and (b) are collected in table 1.

Exciting Cs_2GeF_6: 2% Re^{4+} into Γ_8 (^2E_g) at 10 804 cm^{-1} leads to yellow upconversion luminescence. In figure 4(a) the corresponding upconversion-luminescence spectra are depicted for five different temperatures in comparison to the 15 K luminescence spectrum excited at 19 430 cm^{-1}. The spectra are scaled to identical 17 383 cm^{-1} peak heights. The integrated Γ_7 ($^2T_{2g}$) $\rightarrow$ Γ_8 ($^4A_{2g}$) upconversion-luminescence intensity decreases as indicated with the cross markers in figure 4(b). The circles in figure 4(b) show the temperature dependence of the 10 804 cm^{-1} absorbance to the power of 1.7. This was estimated from the broadening observed in the excitation spectrum of the Γ_8 ($^2T_{1g}$) $\rightarrow$ Γ_8 ($^4A_{2g}$) NIR luminescence, because no suitable absorption spectra in the 10 800 cm^{-1} region could be recorded at elevated temperatures.

The 15 K Cs_2GeF_6: 2% Re^{4+} excitation spectra of the Γ_8 ($^2T_{1g}$) $\rightarrow$ Γ_8 ($^4A_{2g}$) NIR luminescence and the Γ_7 ($^2T_{2g}$) $\rightarrow$ Γ_8 ($^4A_{2g}$) upconversion luminescence detected at 8861 cm^{-1} and 17 383 cm^{-1}, respectively, are shown in figure 5. The two spectra are very similar. They are labelled according to the absorption spectrum published by Lomenzo *et al* [16]. The most intense line, i.e. the ν_6 vibronic origin of Γ_8 (^2E_g) at 10 804 cm^{-1}, was used to excite the upconversion spectra reported in figure 4, see the preceding paragraph.

Semilogarithmic plots of the 15 K Γ_7 ($^2T_{2g}$) $\rightarrow$ Γ_8 ($^4A_{2g}$) and Γ_8 ($^2T_{1g}$) $\rightarrow$ Γ_8 ($^4A_{2g}$) luminescence decays observed for Cs_2GeF_6: 2% Re^{4+} are shown in figures 6(a) and (b),

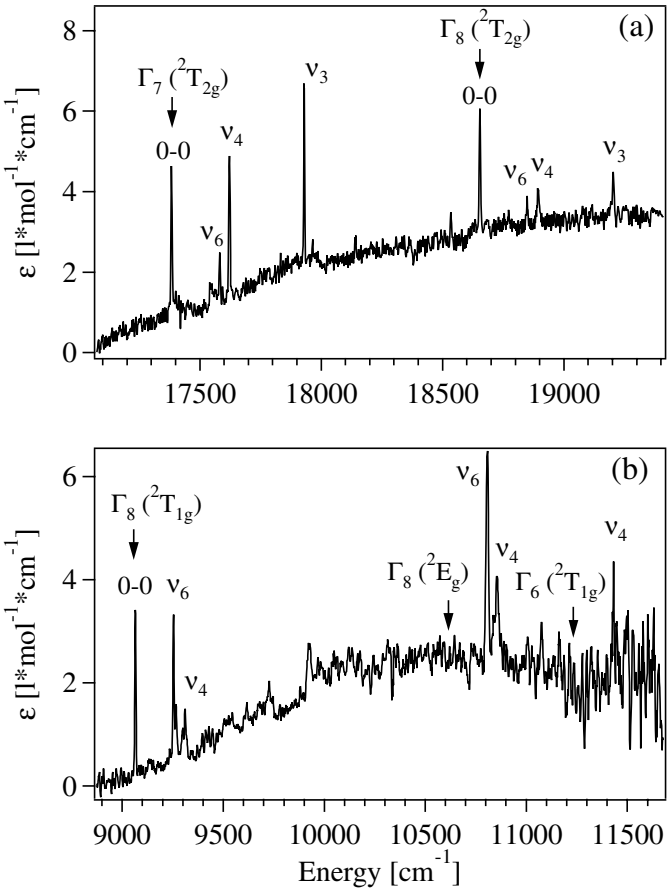

Figure 1. 15 K absorption spectra of Cs_2GeF_6: 2% Re^{4+} in the $^4A_{2g} \rightarrow {}^2T_{2g}$ (a) and $^4A_{2g} \rightarrow {}^2E_g/{}^2T_{1g}$ (b) spectral ranges. 0–0 and ν_i ($i = 3, 4, 6$) denote electronic and vibronic origins, respectively.

respectively. Excitation and detection energies were 18 653 cm^{-1} and 17 138 cm^{-1}, respectively, in (a) and 11 429 cm^{-1} and 8861 cm^{-1}, respectively, in (b). The solid smooth lines represent least-squares fits of functions $a+b\exp(-t/\tau)$ to the experimental data. Thus 15 K lifetimes of 1.3 μs and 610 μs were determined for Γ_7 ($^2T_{2g}$) and Γ_8 ($^2T_{1g}$), respectively. With increasing temperatures, both lifetimes decrease as shown in the insets to figures 6(a) and (b).

The 15 K upconversion-luminescence transient of Cs_2GeF_6: 2% Re^{4+} excited with a 10 ns laser pulse at 11 429 cm^{-1} and detected at 17 138 cm^{-1} is shown as a semilogarithmic plot in figure 7. The upconversion-luminescence decay is non-single exponential. The inset gives an enlarged view of the first 40 μs of the transient, recorded with a better time resolution.

4. Discussion

4.1. Energy-level structure of Cs_2GeF_6: 2% Re^{4+}

The optical absorption, MCD and luminescence spectra of Re^{4+}-doped chloride and bromide lattices have been studied extensively in the past [18–25]. In contrast, the fluoride analogue has

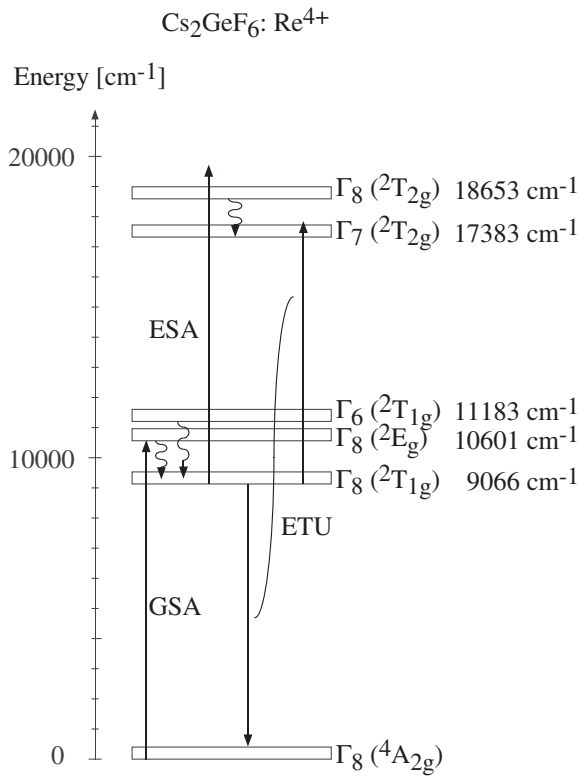

Figure 2. Energy-level scheme of Cs_2GeF_6: 2% Re^{4+} with possible upconversion mechanisms. GSA, ESA and ETU denote ground-state absorption, excited-state absorption and energy-transfer upconversion, respectively. The curly arrows indicate multiphonon-relaxation processes. Origin energies of absorption transitions are given on the right.

received little attention in the literature. The polarized absorption spectra of a K_2ReF_6 single crystal [26] and the absorption of Re^{4+} doped into the cubic Cs_2GeF_6 host have been analysed [16]. So far, the observation of luminescence has only been reported for a concentrated Cs_2ReF_6 crystal [16].

Re^{4+} has a $5d^3$ electron configuration giving rise to a $^4A_{2g}$ ground state in octahedral ligand fields. The most prominent $3d^3$ analogue of Re^{4+} is the Cr^{3+} ion, which has been spectroscopically investigated in numerous materials. In Re^{4+}, the ligand field experienced by the spatially diffuse 5d electrons is so high that the $^4T_{2g}$ and $^4T_{1g}$ bands are shifted far beyond the high-energy edge of the visible spectral range. Consequently, the lowest excited d–d states are the spin-flips ^2E_g, $^2T_{1g}$ and $^2T_{2g}$, which all arise from the same $(t_{2g})^3$ strong-field electron configuration as the $^4A_{2g}$ ground state. The orbitally threefold degenerate states are split by spin–orbit coupling.

According to the literature [16], the sets of sharp lines observed around 10 000 cm^{-1} and 18 000 cm^{-1} in the absorption spectrum depicted in figures 1(b) and (a), respectively, are assigned to Γ_8 ($^2T_{1g}$), Γ_8 (^2E_g), Γ_6 ($^2T_{1g}$) and Γ_7 ($^2T_{2g}$), Γ_8 ($^2T_{2g}$), respectively. The exact origin energies of these spin-flip excited states are given in figure 2, showing a schematic energy-level diagram of the octahedral ReF_6^{2-} chromophore. These energies are significantly higher than those of the analogous $ReCl_6^{2-}$, where the two sets of states are observed around

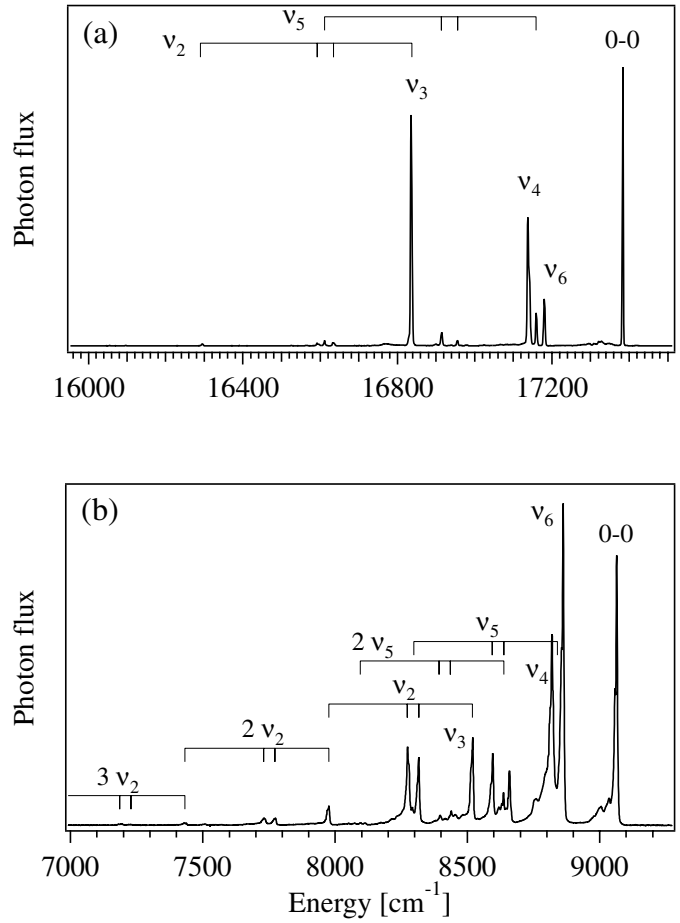

Figure 3. 15 K VIS (a) and NIR (b) luminescence spectra observed in Cs_2GeF_6: 2% Re^{4+} upon excitation at 19 428 cm^{-1} and 10 804 cm^{-1}, respectively. 0–0 and ν_i ($i = 2, 3, 4, 5, 6$) denote electronic and vibronic transitions, respectively.

9000 cm^{-1} and 15 000 cm^{-1}, respectively, as a consequence of the smaller Racah parameters in the latter [12].

The absorption spectra in figures 1(a) and (b) reveal extensive vibronic structure, due to the strict octahedral coordination of Re^{4+} in the Cs_2GeF_6 host, prohibiting electric-dipole (ED) intensity in the electronic origins. Electronic-origin intensity can therefore only be induced by magnetic-dipole (MD) or higher electric-multipole mechanisms. By coupling of the electronic transitions to ungerade modes, ED vibronic intensity is induced. Three normal modes of the octahedral ReF_6^{2-} unit transform ungerade and can thus act as enabling modes, i.e. the ν_6 (t_{2u}) bending and the ν_4 (t_{1u}) and ν_3 (t_{1u}) stretching modes. The most intense features in the absorption spectra displayed in figures 1(a) and (b) can be assigned to the 0–0 electronic origins and the ν_i vibronic origins as indicated. No strong progressions in gerade modes are observed on the electronic and vibronic origins, which is a consequence of the intraconfigurational character of these spin-flip transitions. A more detailed analysis of the Cs_2GeF_6: Re^{4+} absorption spectrum is given in reference [16].

Table 1. Line positions (in cm^{-1}) observed in the 15 K luminescence spectra of Cs_2GeF_6: 2% Re^{4+} depicted in figures 3(a) and (b). The ΔE column contains energy differences to the electronic origins. The last column gives the assignment of the lines and energies (in cm^{-1}) for the vibrational modes.

E (cm^{-1})	ΔE (cm^{-1})	Assignment
17 383	0	Γ_7 ($^2T_{2g}$) → Γ_8 ($^4A_{2g}$)
17 180	203	ν_6 (203)
17 159	224	ν_5 (224)
17 138	245	ν_4 (245)
16 956	427	$\nu_6 + \nu_5$ (224)
16 914	469	$\nu_4 + \nu_5$ (224)
16 836	547	ν_3 (547), ν_2 (547)
16 633	750	$\nu_6 + \nu_2$ (547)
16 611	772	$\nu_3 + \nu_5$ (225)
16 591	792	$\nu_4 + \nu_2$ (547)
16 295	1088	$\nu_3 + \nu_2$ (541), $2\nu_2$ (541)
9064	0	Γ_8 ($^2T_{1g}$) → Γ_8 ($^4A_{2g}$)
8861	203	ν_6 (203)
8819	245	ν_4 (245)
8659	405	
8636	428	$\nu_6 + \nu_5$ (223)
8595	469	$\nu_4 + \nu_5$ (224)
8519	545	ν_3(545), ν_2 (545)
8440	624	$\nu_6 + 2\nu_5$ (196)
8397	667	$\nu_4 + 2\nu_5$ (198)
8316	748	$\nu_6 + \nu_2$ (545)
8292	772	$\nu_3 + \nu_5$ (225)
8274	790	$\nu_4 + \nu_2$ (545)
7976	1088	$\nu_3 + \nu_2$ (541), $2\nu_2$ (541)
7775	1289	$\nu_6 + 2\nu_2$ (541)
7730	1334	$\nu_4 + 2\nu_2$ (544)
7430	1634	$\nu_3 + 2\nu_2$ (546), $3\nu_2$ (546)
7228	1836	$\nu_6 + 3\nu_2$ (547)
7190	1874	$\nu_4 + 3\nu_2$ (540)

The weak electron–phonon coupling of the spin-flip excited states greatly reduces the efficiency of multiphonon relaxation. The situation encountered in Cs_2GeF_6: 2% Re^{4+} is thus similar to f–f excited states in lanthanides, in which the rate constants of multiphonon-relaxation processes k_{mp} are well modelled by the energy-gap law [27, 28]:

$$k_{mp} = \beta \cdot e^{-\alpha p} \tag{1}$$

where β and α are parameters typical for the material and $p = \Delta E/\hbar\omega_{max}$ corresponds to the energy gap ΔE between the luminescent state and the next-lower energy state in units of the largest vibrational energy quantum $\hbar\omega_{max}$. In lanthanides, luminescence is typically observed for $p > 5$ [2]. $\hbar\omega_{max}$ is around 600 cm^{-1} in Cs_2GeF_6: Re^{4+} [16]. This leads to $p < 3$ values for Γ_6 ($^2T_{1g}$), Γ_8 (^2E_g) and Γ_8 ($^2T_{2g}$) (see figure 2) and consequently these states relax very efficiently to the next lower states. Γ_8 ($^2T_{1g}$) and Γ_7 ($^2T_{2g}$) are separated from lower electronic states by energy gaps corresponding to $p = 15$ and $p = 10$, respectively, and are thus expected to show luminescence. The dependence of multiphonon relaxation-rate constants on the maximum vibrational frequency $\hbar\omega_{max}$ of Re^{4+}-doped halide lattices is well illustrated by the observation of Γ_8 ($^2T_{2g}$) luminescence in Cs_2SnBr_6: Re^{4+}, which is

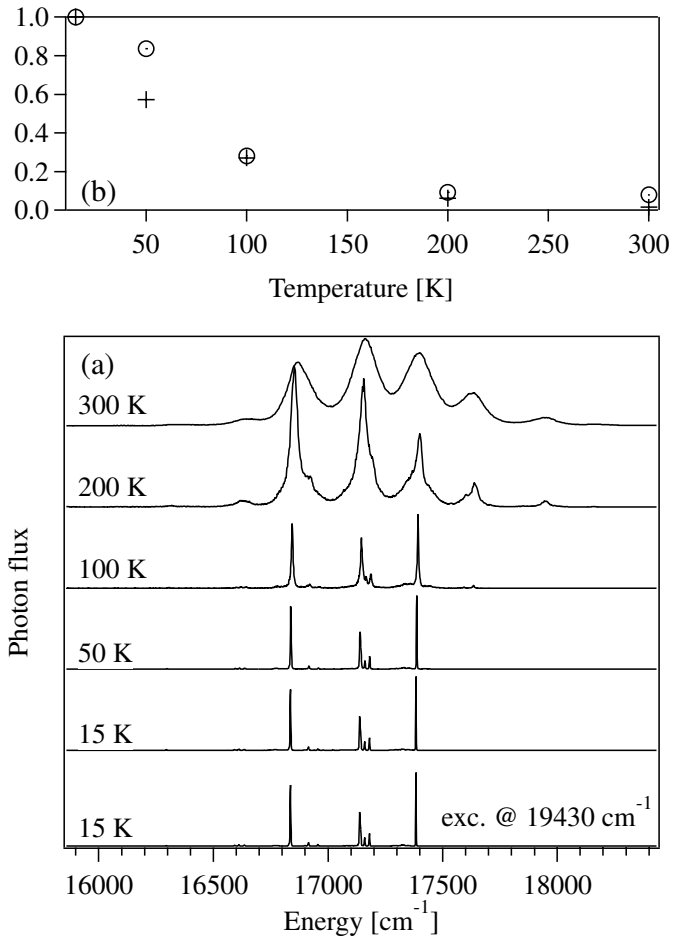

Figure 4. Temperature dependence of the upconversion luminescence observed in Cs_2GeF_6: 2% Re^{4+} upon 10 804 cm^{-1} excitation. (a) shows the upconversion-luminescence spectra measured at the indicated temperatures and scaled to identical 17 383 cm^{-1} peak heights. The 15 K luminescence spectrum excited at 19 430 cm^{-1} is shown at the bottom. (b) compares the integrated upconversion-luminescence intensity (+) with the 10 804 cm^{-1} absorbance to the power of 1.7 (◯). Both plots are normalized with respect to their 15 K values.

separated by an energy gap from Γ_7 ($^2T_{2g}$) corresponding to $p = 8$ in this host with $\hbar\omega_{max} = 220$ cm^{-1} [22, 25]. In chloride analogues, on the other hand, with $\hbar\omega_{max} = 350$ cm^{-1} the energy gap between the same two states corresponds to $p = 4$, leading to a predominantly non-radiative relaxation of Γ_8 ($^2T_{2g}$) [12].

In pure Cs_2ReF_6 with Re^{4+} occupying D_{3d} sites, visible luminescence assigned to Γ_7 ($^2T_{2g}$) $\rightarrow \Gamma_8$ ($^4A_{2g}$) (O_h notation) has been reported [16] This luminescence transition around 17 000 cm^{-1} is also observed in the diluted Cs_2GeF_6: 2% Re^{4+} sample upon 19 430 cm^{-1} excitation into Γ_8 ($^2T_{2g}$) (see figure 3(a)). Exciting Cs_2GeF_6: 2% Re^{4+} into Γ_8 (^2E_g) at 10 804 cm^{-1} induces the Γ_8 ($^2T_{1g}$) $\rightarrow \Gamma_8$ ($^4A_{2g}$) NIR luminescence around 9000 cm^{-1}, as shown in figure 3(b). Since the luminescence spectra of the ReF_6^{2-} chromophore diluted in Cs_2GeF_6 reported here are much more highly resolved than those

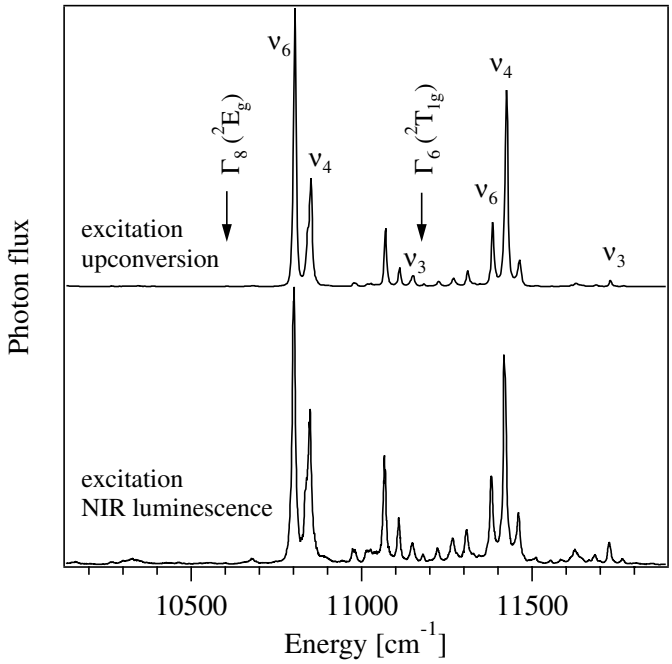

Figure 5. 15 K excitation spectra of the Cs_2GeF_6: 2% Re^{4+} upconversion and NIR luminescence transitions detected at 17 383 cm^{-1} and 8861 cm^{-1}, respectively. The electronic origins of $\Gamma_8\,(^4A_{2g}) \rightarrow \Gamma_8\,(^2E_g)$ and $\Gamma_6\,(^2T_{1g})$ and the vibronic origins involving ν_6 (t_{2u}), ν_4 (t_{1u}) and ν_3 (t_{1u}) modes are assigned.

of Cs_2ReF_6 in reference [16] and since our host lattice provides an exactly octahedral site, we now present a detailed analysis of the fine structure of the two luminescence bands in figure 3.

The $\Gamma_7\,(^2T_{2g}) \rightarrow \Gamma_8\,(^4A_{2g})$ transition is MD allowed, leading to the observation of the electronic origin 0–0 at 17 383 cm^{-1}, as shown in figure 3(a). The lines separated by 203 cm^{-1}, 245 cm^{-1} and 547 cm^{-1} from the electronic origin are assigned to the vibronic origins involving one quantum of the ν_6 (t_{2u}), ν_4 (t_{1u}) and ν_3 (t_{1u}) enabling modes, respectively. These frequencies compare well with the vibrational frequencies of 181 cm^{-1}, 249 cm^{-1} and 535 cm^{-1} determined in Cs_2ReF_6 for the corresponding modes [16]. No splitting of the threefold degenerate modes was observed in Cs_2ReF_6, despite the lower site symmetry of D_{3d}. The vibronic origin involving the ν_3 (t_{1u}) stretch vibration is more intense than the vibronic origins involving the ν_4 (t_{1u}) and ν_6 (t_{2u}) bending vibrations, in agreement with the analogous spectrum of Cs_2ReF_6 [16]. The pattern of the electronic and vibronic origins is repeated at 224 cm^{-1} and 547 cm^{-1} to lower energy, corresponding to the first members in a progression involving the ν_5 (t_{2g}) and ν_2 (e_g) modes. This is indicative of a Jahn–Teller (JT) effect in the $^2T_{2g}$ excited state. The $^4A_{2g}$ ground state is JT stable as its degeneracy, to first order, arises from the spin-degeneracy only. The progressions in the ν_5 (t_{2g}) and ν_2 (e_g) JT modes are very short with corresponding Huang–Rhys factors of $S \approx 0.1$ and $S \approx 0.02$, respectively. Interestingly, there are no sidebands involving the totally symmetric ν_1 (a_{1g}) vibration, indicating extremely small Huang–Rhys parameters. The small Huang–Rhys parameters are in agreement with the intraconfigurational nature of the $\Gamma_7\,(^2T_{2g}) \rightarrow \Gamma_8\,(^4A_{2g})$ transition.

Also the $\Gamma_8\,(^2T_{1g}) \rightarrow \Gamma_8\,(^4A_{2g})$ transition is MD allowed, leading to the observation of the electronic origin 0–0 at 9066 cm^{-1} (see figure 3(b)). The lines separated by 203 cm^{-1},

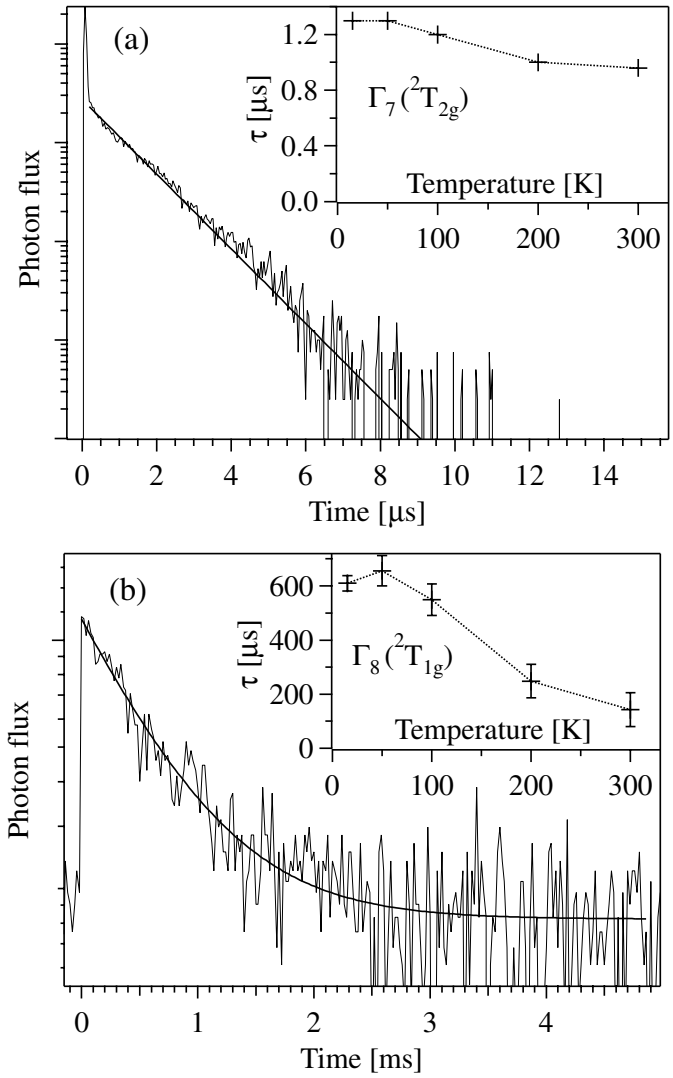

Figure 6. Semilogarithmic plots of the 15 K Cs_2GeF_6: 2% Re^{4+} Γ_7 ($^2T_{2g}$) $\rightarrow$ Γ_8 ($^4A_{2g}$) (a) and the Γ_8 ($^2T_{1g}$) $\rightarrow$ Γ_8 ($^4A_{2g}$) (b) luminescence decays excited with 10 ns laser pulses. Excitation and detection energies were 18 653 cm^{-1} and 17 138 cm^{-1}, respectively, in (a) and 11 429 cm^{-1} and 8861 cm^{-1}, respectively, in (b). The solid smooth lines are functions $a + b\exp(-t/\tau)$. The lifetimes τ of Γ_7 ($^2T_{2g}$) and Γ_8 ($^2T_{1g}$) are plotted in the insets to (a) and (b), respectively.

245 cm^{-1} and 545 cm^{-1} from the electronic origin are assigned to the ν_6 (t_{2u}), ν_4 (t_{1u}) and ν_3 (t_{1u}) vibronic origins, respectively. Within experimental accuracy, these energies are identical to the values determined for the Γ_7 ($^2T_{2g}$) $\rightarrow$ Γ_8 ($^4A_{2g}$) transition discussed above. That is what we expect for luminescence transitions involving the same final level. Compared to the Γ_7 ($^2T_{2g}$) $\rightarrow$ Γ_8 ($^4A_{2g}$) transition, the relative intensities of the vibronic origins are different. The ν_6 (t_{2u}) vibronic origin is the most intense line in the Γ_8 ($^2T_{1g}$) $\rightarrow$ Γ_8 ($^4A_{2g}$) spectrum, whereas it is the weakest one in Γ_7 ($^2T_{2g}$) $\rightarrow$ Γ_8 ($^4A_{2g}$). The same was observed in the analogous transitions of Cs_2ZrCl_6: Re^{4+} [12]. Two members of a progression in the

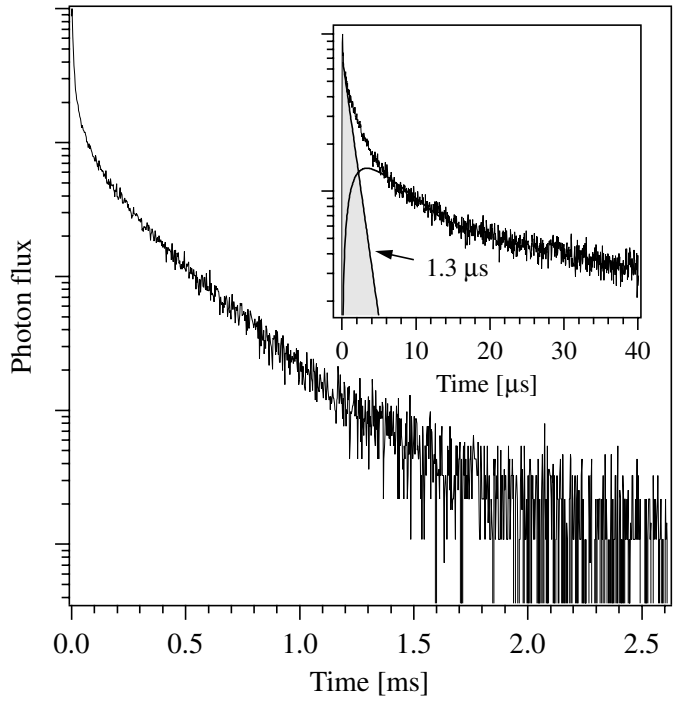

Figure 7. Semilogarithmic plot of the 15 K Cs_2GeF_6: 2% Re^{4+} upconversion-luminescence transient excited at $t = 0$ with a 10 ns laser pulse. Excitation and detection energies were 11 429 cm^{-1} and 17 138 cm^{-1}, respectively. The inset shows the first 40 μs of the transient and the shaded area represents a single-exponential decay with $\tau = 1.3$ μs. The smooth curved line is a fit of equation (2) to the first 15 μs of the difference between the experimental transient and the single exponential decay.

ν_5 (t_{2g}) mode ($S \approx 0.2$) and at least three members of a progression in the ν_2 (e_g) mode ($S \approx 0.3$) with energy intervals of 224 cm^{-1} and 545 cm^{-1}, respectively, are observed on the electronic and vibronic origins of the Γ_8 ($^2T_{1g}$) $\rightarrow$ Γ_8 ($^4A_{2g}$) transition. The progressions in these JT modes are thus significantly longer than those observed in the Γ_7 ($^2T_{2g}$) $\rightarrow$ Γ_8 ($^4A_{2g}$) transition. Again, no ν_1 (a_{1g}) sidebands are observed.

4.2. Upconversion mechanisms

Exciting Cs_2GeF_6: 2% Re^{4+} into Γ_8 (^2E_g) at 10 804 cm^{-1} leads to the observation of yellow upconversion luminescence (see figure 4). This is assigned to the Γ_7 ($^2T_{2g}$) $\rightarrow$ Γ_8 ($^4A_{2g}$) transition by comparison with the luminescence spectrum of Cs_2GeF_6: 2% Re^{4+} observed upon 19 430 cm^{-1} excitation. For a discussion of the Cs_2GeF_6: 2% Re^{4+} upconversion it is necessary to introduce two upconversion mechanisms, GSA/ESA and GSA/ETU, and briefly discuss their experimentally accessible fingerprints. GSA, ESA and ETU stand for ground-state absorption, excited-state absorption and energy-transfer upconversion, respectively.

The GSA/ETU and GSA/ESA mechanisms can be distinguished in CW and pulsed experiments as follows. In the GSA/ETU mechanism the actual upconversion step occurs by energy transfer between two ions that have both been excited to their intermediate excited states by GSA. This energy transfer promotes one of the ions to a higher excited state, whereas the other ion relaxes to an energetically lower lying state. GSA/ETU is characterized

by a resemblance of the upconversion-excitation spectrum and the GSA spectrum. In pulsed excitation experiments, the GSA/ETU mechanism is characterized by upconversion-luminescence transients consisting of a rise followed by a decay period. This is a consequence of the relatively slow feeding of the emitting state by the energy-transfer step.

In case of a GSA/ESA mechanism, the upconversion is induced by sequential absorption steps, usually on a single ion, i.e. GSA to an intermediate state, followed by ESA to a higher excited state. Here, the upconversion-excitation spectrum contains both GSA and ESA features. Upon short-pulse excitation, the upconversion-luminescence transient decays with the lifetime of the upper excited state. This decay starts immediately after the end of the excitation pulse, reflecting the fact that both sequential excitation steps occur during the laser pulse.

In Cs_2GeF_6: 2% Re^{4+} at 15 K the initial 10 804 cm^{-1} excitation into Γ_8 (^2E_g) is followed by very rapid multiphonon relaxation to Γ_8 ($^2T_{1g}$) (see curly arrow in figure 2). The second step in the upconversion sequence thus always starts from Γ_8 ($^2T_{1g}$), irrespective of the mechanism and the originally excited state within the $^2E_g/^2T_{1g}$ multiplet. From the Γ_8 ($^2T_{1g}$) intermediate state at 9066 cm^{-1}, the Γ_7 ($^2T_{2g}$) and Γ_8 ($^2T_{2g}$) states at 17 383 cm^{-1} and 18 653 cm^{-1} can in principle be reached by ESA or ETU mechanisms, as discussed in detail below.

The energy-level scheme depicted in figure 2 indicates that ESA at the 10 804 cm^{-1} excitation energy is expected to be inefficient, as it is higher by 1217 cm^{-1} than the energy difference between Γ_8 ($^2T_{1g}$) and Γ_8 ($^2T_{2g}$). The energetic situation looks more favourable for an ETU process starting from Γ_8 ($^2T_{1g}$) and ending in Γ_7 ($^2T_{2g}$) (see right-hand side of figure 2).

The upconversion-excitation spectrum also indicates a GSA/ETU mechanism (see figure 5) in which the excitation spectra of the Γ_7 ($^2T_{2g}$) $\rightarrow$ Γ_8 ($^4A_{2g}$) upconversion luminescence and the Γ_8 ($^2T_{1g}$) $\rightarrow$ Γ_8 ($^4A_{2g}$) NIR luminescence are compared. The upconversion-excitation spectrum does not contain any new features and significant GSA/ESA contributions can thus be ruled out. As the GSA/ETU mechanism involves two GSA steps the upconversion-excitation spectrum is expected to correspond to the square of the excitation spectrum of the NIR luminescence. Figure 5 reveals a non-linear relationship between the relative intensities of the two excitation spectra. A more detailed analysis shows that the upconversion-excitation spectrum roughly corresponds to the excitation spectrum of the NIR luminescence taken to the power of 1.7. This is the power dependence experimentally determined for the upconversion intensity in the power range of this experiment.

At first sight, the upconversion-luminescence transient shown in figure 7 contradicts a GSA/ETU mechanism. It does not show a rise part, even under the increased time resolution depicted in the inset to figure 7. This is the typical signature of a GSA/ESA mechanism. A closer inspection of the transient reveals a non-single exponential decay with components in the range from 1.9 μs to 270 μs. This is significantly longer than the lifetime $\tau = 1.3$ μs determined from figure 6(a) at 15 K for the emitting state. This proves that the emitting state Γ_7 ($^2T_{2g}$) is fed from a long-lived population storage reservoir during several hundred microseconds after the excitation pulse. In Cs_2GeF_6: 2% Re^{4+} at 15 K only an ETU process starting from the long-lived Γ_8 ($^2T_{1g}$) with $\tau = 610$ μs can provide this prolonged excitation.

We conclude that the upconversion-luminescence transient is dominated by a GSA/ETU transient with a minor GSA/ESA contribution in the first 5 μs. This is shown by the two smooth lines in the inset to figure 7. The initial population in Γ_7 ($^2T_{2g}$) is exclusively caused by a GSA/ESA mechanism. This initial population decays exponentially with the 15 K Γ_7 ($^2T_{2g}$) lifetime of 1.3 μs. It corresponds to the integral $\int I_0 \exp(-t/1.3\ \mu\text{s})\, dt$, visualized by the shaded area in the inset to figure 7. We obtain a GSA/ESA contribution of 10% to the total integrated upconversion-luminescence intensity. Thus the GSA/ETU contribution is

also dominant for pulsed excitation. Its time evolution is obtained by subtracting the shaded part from the experimental transient in the inset to figure 7.

In dimeric systems the temporal behaviour of the upconversion-luminescence intensity I induced by a GSA/ETU mechanism upon pulsed excitation is described by [17]

$$I(t) = a \cdot (e^{-t \cdot k_1} - e^{-t \cdot k_2}) \tag{2}$$

where $k_1 = 2/\tau_1 + w_{ETU}$ is related to the intermediate state lifetime τ_1 and the ETU rate constant w_{ETU}, and $k_2 = 1/\tau_2$ is the inverse of the emitting state lifetime. This is only a rough approximation for our system, since the Re^{4+} ions are statistically distributed and energy migration is possible. It nevertheless provides a reasonable basis for the following order-of-magnitude estimate.

The smooth curved line in figure 7 was obtained by fitting equation (2) to the first 15 μs of the GSA/ETU part of the upconversion-luminescence transient. This fraction of the curve is probably characteristic of ETU between excited nearest Re^{4+} neighbours in the Cs_2GeF_6: 2% Re^{4+} crystal. It has a rise time $1/k_2 = 1.4$ μs that compares very well with the 15 K Γ_7 ($^2T_{2g}$) lifetime of $\tau_1 = 1.3$ μs. $1/k_1 = 12$ μs is significantly shorter than the intermediate state lifetime $\tau_1 = 610$ μs, thus indicating that w_{ETU} dominates k_1 in equation (2). In other words, the decay part of the transient in figure 7 is mainly determined by the ETU rate. For nearest-neighbour Re^{4+} pairs at 15 K w_{ETU} has a value of 8×10^4 s. With increasing delay after the laser pulse ETU processes between more distant Re^{4+} neighbours determine the decay, leading to the observed slowing down in figure 7.

The analysis of the upconversion processes in Cs_2ZrCl_6: 2.5% Re^{4+} revealed that in this system they are exclusively due to ETU [12]. This observation was attributed to an exceptionally efficient ETU. In contrast to our results in the title compound presented above, the rise part of the upconversion-luminescence transients of Cs_2ZrCl_6: 2.5% Re^{4+} excited with 10 ns excitation pulses at 1064 nm was not masked by an initial GSA/ESA part.

4.3. Efficiency of NIR to VIS upconversion

The analysis of the Cs_2ZrCl_6: 2.5% Re^{4+} system revealed intermediate and upper excited-state decay times that were essentially radiative over the whole temperature range from 10 K to room temperature [12]. The upconversion was found to be very efficient, and under moderate steady-state pumping conditions, it was the main mechanism for depletion of the intermediate excited-state population. Potential upconversion-laser schemes were proposed on the basis of these promising spectroscopic results [12].

With the present study, we extend the Re^{4+} upconversion research to fluorides. This extension is mainly motivated by the favourable physical and chemical properties of fluorides which make them common hosts in laser and phosphor-material related research. In the following we analyse the efficiency of NIR to VIS upconversion in our system.

The temperature dependence of the yellow upconversion luminescence in Cs_2GeF_6: 2% Re^{4+} is shown in figure 4(a). With increasing temperature, the luminescence lines broaden significantly. The upconversion luminescence is observed up to room temperature, but the integrated Γ_7 ($^2T_{2g}$) $\rightarrow$ Γ_8 ($^4A_{2g}$) upconversion-luminescence intensity upon monochromatic laser excitation at 10 804 cm^{-1} steadily decreases with increasing temperature (see cross markers in figure 4(b)). The room temperature upconversion-luminescence intensity is only 2% of the value observed at 15 K.

Figure 4(b) also shows the temperature dependence of the 10 804 cm^{-1} absorbance to the power of 1.7 that was estimated from the temperature dependence of the NIR-luminescence excitation spectra. Within experimental accuracy, the two plots in figure 4(b) represent

the same temperature dependence. We conclude that the decrease of the upconversion-luminescence intensity with increasing temperature is mainly due to the decreasing excitation efficiency at 10 804 cm^{-1} and not to a decrease of the upconversion efficiency. For broad-band excitation an essentially constant upconversion-luminescence intensity up to room temperature can be expected.

The 15 K lifetimes of Γ_8 ($^2T_{1g}$) and Γ_7 ($^2T_{2g}$) are 610 μs and 1.3 μs, respectively. By comparing these measured values with calculated radiative lifetimes, we can estimate the contribution of non-radiative relaxation to the overall excited-state population decay. The radiative lifetime τ_{rad} and the corresponding decay-rate constant k_{rad} are related, by equation (3), to the oscillator strength f of the corresponding transition [29]:

$$1/k_{rad} = \tau_{rad} = \alpha \frac{\lambda_{eg}^2}{n[(n^2+2)/3]^2} \frac{g_e}{g_g} \frac{1}{f}. \tag{3}$$

α is a constant (1.5×10^4 s m^{-2}), λ_{eg} is the average emission wavelength, g_g and g_e are the degeneracies of the ground and excited states, respectively, and $n = 1.42$ is the refractive index of Cs_2GeF_6 [30]. Based on the 15 K absorption spectrum depicted in figure 1(b), the calculated 15 K radiative lifetime of Γ_8 ($^2T_{1g}$) is $\tau_{rad} = 9.1$ ms.

The situation is more complicated for the Γ_7 ($^2T_{2g}$) emitting state, because luminescence transitions to several final states are possible. Only the decay-rate constant of the transition to the ground state can be obtained from the absorption spectrum, and using equation (3) we get $k_{rad} = 670$ s^{-1} for Γ_7 ($^2T_{2g}$) $\rightarrow$ Γ_8 ($^4A_{2g}$) at 15 K. The decay-rate constants of the inter-excited state luminescence transitions, i.e. Γ_7 ($^2T_{2g}$) $\rightarrow$ Γ_8 ($^2T_{1g}$), Γ_8 (^2E_g), Γ_6 ($^2T_{1g}$) were estimated as follows. In the related system Cs_2ZrCl_6: 2.5% Re^{4+} the sum of the rate constants of these latter transitions was found to be three times larger than the Γ_7 ($^2T_{2g}$) $\rightarrow$ Γ_8 ($^4A_{2g}$) rate constant [12]. This observation was attributed to the effects of spin-selection rules and state multiplicities, favouring the inter-excited state doublet $\rightarrow$ doublet transitions. Assuming the same in Cs_2GeF_6: 2% Re^{4+} we obtain a calculated $\tau_{rad} = 370$ μs for Γ_7 ($^2T_{2g}$) at 15 K.

Both calculated radiative lifetimes $\tau_{rad} = 370$ μs and $\tau_{rad} = 9.1$ ms are significantly longer than the observed 15 K lifetimes $\tau = 1.3$ μs and $\tau = 610$ μs of Γ_7 ($^2T_{2g}$) and Γ_8 ($^2T_{1g}$), respectively. This indicates that non-radiative processes account for 99.6% and 93.3% of the excited-state decays, respectively, at 15 K. Based on the arguments given in section 4.1, multiphonon relaxation is unlikely for both these states in the ReF_6^{2-} chromophore. Also cross-relaxations can be excluded for both states. Energy migration to killer traps thus represents the most likely efficient non-radiative de-excitation pathway for Γ_7 ($^2T_{2g}$) and Γ_8 ($^2T_{1g}$) in our samples.

These impurity traps are most likely related to the presence of OH^- in the host lattice. OH^- is known to substitute very easily for F^- in fluoride crystals and glasses and thus represents a major problem in light emitting materials [31]. With its high frequency stretching mode of roughly 3500 cm^{-1}, the OH^- group induces multiphonon relaxation across very large energy gaps. Our Cs_2GeF_6: 2% Re^{4+} crystals were grown from aqueous solution, and an incorporation of OH^- into the host lattice appears likely in this process.

Some OH^- impurity was presumably already contained in the K_2ReF_6 starting material used to grow the Cs_2GeF_6: 2% Re^{4+} crystals. This compound was slightly pink which, according to Weise [15], is indicative of a partial substitution of F^- by OH^-. The Re^{4+} ions containing OH^- in their coordination sphere might thus represent the killer traps in our crystal. The Re^{4+} concentration of 2% in our crystal is sufficient to guarantee efficient energy migration to these traps at all temperatures.

The temperature dependences of the Γ_7 ($^2T_{2g}$) and Γ_8 ($^2T_{1g}$) lifetimes are shown in the insets to figures 6(a) and (b), respectively. The Γ_7 ($^2T_{2g}$) lifetime is only slightly reduced

from 1.3 μs at 15 K to 1.0 μs at room temperature, whereas the Γ_8 ($^2T_{1g}$) lifetime decreases from 610 μs at 15 K to 150 μs at room temperature.

The above analysis shows that a major part of the excited-state population is lost via non-radiative relaxation. Therefore, the overall upconversion efficiency, i.e. the ratio of emitted yellow photons to absorbed NIR photons, is low in our crystal. We must emphasize that this is not caused by an inefficient upconversion step, but rather by loss processes preceding and following it. Therefore, improving the overall upconversion efficiency in Cs_2GeF_6: 2% Re^{4+} is mainly a question of reducing these losses.

5. Conclusions

We have synthesized Cs_2GeF_6: 2% Re^{4+} and analysed its optical energy-level structure. Compared to the isostructural Cs_2ZrCl_6: 2.5% Re^{4+}, the $^2E_g/^2T_{1g}$ intermediate and $^2T_{2g}$ upper excited states are shifted to higher energy by 1400 cm^{-1} and 3500 cm^{-1}, respectively. The $^2E_g/^2T_{1g}$ intermediate states thus occur in the 9000 cm^{-1} to 12 000 cm^{-1} energy region, where they are more easily accessible to Ti:Sapphire laser excitation. Upon excitation at 10 804 cm^{-1}, yellow Γ_7 ($^2T_{2g}$) $\rightarrow$ Γ_8 ($^4A_{2g}$) upconversion luminescence is observed over the whole temperature range from 15 K up to room temperature.

So far, the upconversion efficiency achieved in our crystals is low due to non-radiative loss processes depopulating both the intermediate and the upper excited state. These loss processes are believed to be due to the presence of OH^- impurities in the crystal. Thus, reducing the OH^- content in our fluoride crystals should lead to a substantial increase of the overall upconversion efficiency. Improving the efficiency of the ReF_6^{2-} upconversion system is thus primarily a chemical task. As the ternary A_2GeF_6 (A = alkali ion) compounds tend to liberate GeF_4 at higher temperatures, it is not trivial to grow Cs_2GeF_6 from the melt.

In preliminary experiments, we have observed upconversion emission even in concentrated K_2ReF_6 crystals, demonstrating that the ReF_6^{2-} upconversion can be observed over a very wide concentration range. Exploring the concentration coordinate might thus represent a route to further optimize the ReF_6^{2-} upconversion.

A point to be addressed in the future is the low absorbance of the ReF_6^{2-} chromophore around 10 000 cm^{-1}. An obvious way to increase the absorbance involves the use of sensitizers such as Yb^{3+}. Yb^{3+} with its excited states slightly above 10 000 cm^{-1} has successfully been used as a sensitizer for lanthanide-ion upconversion systems and might also be suitable as a sensitizer for the ReF_6^{2-} system. Host sensitization involving crystalline hosts such as Cs_2NaYbF_6 appears to be especially promising, in view of the results recently achieved in the analogous $Cs_2NaYbCl_6$: Re^{4+} system [32].

More materials-oriented research might be directed towards the use of fluoride glasses as hosts for the ReF_6^{2-} chromophore. Heavy-metal fluoride glasses such as ZBLAN, composed of 54% ZrF_4, 20% BaF_2, 4% LaF_3, 2% NaF and 3% AlF_3 contain octahedrally coordinated sites that might be partially doped with ReF_6^{2-}. Heavy-metal fluoride glasses are attractive materials for many optical applications due to their wide range of transparency from 250 nm in the UV to 7.5 μm in the infrared, small thermal dependence of the optical properties and ease of cutting and polishing [33].

Acknowledgments

Financial support by the Swiss National Science Foundation is gratefully acknowledged.

References

[1] Auzel F E 1973 *Proc. IEEE* **61** 758
[2] Riedener T, Krämer K W and Güdel H U 1995 *Inorg. Chem.* **34** 2745
[3] Lüthi S R, Pollnau M, Güdel H U and Hehlen M P 1999 *Phys. Rev.* B **60** 162
[4] Gamelin D R and Güdel H U 2000 *Acc. Chem. Res.* **33** 235
[5] Kasha M 1950 *Discuss. Faraday Soc.* **9** 14
[6] Jacobsen S M and Güdel H U 1989 *J. Lumin.* **43** 125
[7] May P S and Güdel H U 1991 *J. Chem. Phys.* **95** 6343
[8] Oetliker U, Riley M J, May P S and Güdel H U 1991 *Coord. Chem. Rev.* **111** 125
[9] Wenger O S and Güdel H U 2001 *Inorg. Chem.* **40** 157
[10] Gamelin D R and Güdel H U 1998 *J. Am. Chem. Soc.* **120** 12 143
[11] Gamelin D R and Güdel H U 2000 *J. Phys. Chem.* B **104** 10 222
[12] Gamelin D R and Güdel H U 1999 *Inorg. Chem.* **38** 5154
[13] Wermuth M and Güdel H U 1999 *J. Am. Chem. Soc.* **121** 10 102
[14] Wermuth M and Güdel H U 2001 *J. Chem. Phys.* **114** 1393
[15] Weise E 1956 *Z. Anorg. Allg. Chem.* **283** 377
[16] Lomenzo J, Patterson H, Strobridge S and Engstrom H 1980 *Mol. Phys.* **40** 1401
[17] Buisson R and Vial J C 1981 *J. Phys. Lett. (Paris)* **42** L115
[18] Dorain P B and Wheeler R G 1966 *J. Chem. Phys.* **45** 1172
[19] Collingwood J C, Piepho S B, Schwartz R W, Dobosh P A, Dickinson J R and Schatz P N 1975 *Mol. Phys.* **29** 793
[20] Yoo R K, Lee S C, Kozikowski B A and Keiderling T A 1987 *Chem. Phys.* **117** 237
[21] Black A M and Flint C D 1977 *J. Chem. Soc., Faraday Trans. 2* **73** 877
[22] Flint C D and Paulusz A G 1979 *Chem. Phys. Lett.* **62** 259
[23] Black A M and Flint C D 1979 *J. Mol. Spec.* **70** 481
[24] Flint C D and Paulusz A G 1981 *Mol. Phys.* **43** 321
[25] Black A M and Flint C D 1975 *J. Chem. Soc., Faraday Trans. 2* **71** 1871
[26] Bettinelli M, di Sipio L, Ingletto G, Montenero A and Flint C D 1985 *Mol. Phys.* **56** 1033
[27] Englman R and Jortner J 1970 *Mol. Phys.* **18** 145
[28] van Dijk J M F and Schuurmans M F H 1983 *J. Chem. Phys.* **78** 5317
[29] Imbusch G F and Kopelman R 1981 *Laser Spectroscopy of Solids* ed W M Yen and P M Selzer (Berlin: Springer)
[30] Schuetz W 1936 *Z. Phys. Chem.* B **31** 292
[31] France P W, Carter S F, Day C R and Moore W M 1989 *Fluoride Glasses* ed Alan E Comyns (New York: Wiley)
[32] Gamelin D R and Güdel H U to be submitted.
[33] Mazé G 1989 *Fluoride Glasses* ed Alan E Comyns (New York: Wiley)